Applied Clay Science 180 (2019) 105190

Contents lists available at ScienceDirect

Applied Clay Science

journal homepage: www.elsevier.com/locate/clay

Research Paper

Ethylene glycol monoethyl ether adsorption by interlayer montmorilonite-organic matter complexes: Dependence on the organic matter content and its alkyl chain length

Hongling Bu[a,b], Dong Liu[a,b,*], Peng Yuan[a,b], Xiang Zhou[a,b], Hongmei Liu[a,b], Hongzhe Song[a,b], Baifa Zhang[a,b]

[a] CAS Key Laboratory of Mineralogy and Metallogeny, Guangdong Provincial Key Laboratory of Mineral Physics and Materials, Guangzhou Institute of Geochemistry, Institutions of Earth Science, Chinese Academy of Sciences, Guangzhou 510640, China
[b] University of Chinese Academy of Sciences, Beijing 100049, China

ARTICLE INFO

Keywords:
Montmorillonite
OM
Clay-OM complex
EGME adsorption
TSSA

ABSTRACT

The ethylene glycol monoethyl ether (EGME) adsorption method is an essential and available technique for measuring the total specific surface area (TSSA) of natural rock samples that usually contain an abundant amount of clay-organic matter (clay-OM) complexes. Occurrence sites and types of OM are believed to influence the EGME adsorption behaviors of clay-OM complexes. However, the influence of OM properties on the EGME adsorption mechanism remains unclear until now. In this study, interlayer montmorillonite (Mt)-OM complexes were prepared using the intercalation of OM with various contents and different length of alkyl chains, such as tetramethylammonium bromide (TMAB) and dodecyl trimethyl ammonium bromide (DTAB), based on the cation exchange. EGME adsorption experiments were performed on Mt, OM, and Mt-OM complexes. X-ray diffraction (XRD) and Fourier transform infrared spectroscopy (FTIR) were used to characterize the structural properties of the samples before and after EGME adsorption. The EGME adsorption capacities and the corresponding TSSA decreased after OM intercalation into the interlayer space of Mt. The OM content and the amounts of alkyl chains significantly affected the EGME adsorption behaviors of Mt-OM complexes. For short alkyl chain OM (TMAB), TSSA values of the Mt-OM complexes decreased with the increase of the interlayer OM content. However, for long alkyl chain OM (DTAB), the TSSA values showed a different variation tendency where the smallest TSSA did not appear in the Mt-OM complex with the highest DTAB content. The initial interlayer distance of Mt-OM complexes and the arrangement of interlayer OM are the primarily factors for EGME adsorption behaviors of the Mt-OM complexes. The large initial interlayer distance favored for incremental expansion of Mt. after EGME adsorption, which promoted EGME molecules entering into the interlayer space. The influence of the arrangement of interlayer OM are primarily involved in some newly formed micropores preventing EGME molecules from entering and more adsorption sites were occupied by OM with a higher ordered mode for the conformation of the alkyl chain and a higher packing density for the arrangement.

1. Introduction

The ethylene glycol monoethyl ether (EGME) adsorption method is an essential technique for measuring the specific surface area (SSA) of natural samples. In contrast to the N_2 molecule, EGME molecules can enter the internal surface of minerals, such as the interlayer surface of swelling montmorillonite and detect the area of such an internal surface (Carter et al., 1965; Pennell et al., 1995; Cerato and Lutenegger, 2002; Yukselen and Kaya, 2006; Arnepalli et al., 2008; Bayat et al., 2015). The obtained SSA based on the EGME adsorption method is thus believed to be the total specific surface area (TSSA). The EGME adsorption method has been used for the TSSA measurement of the various clay-based natural samples, such as clay minerals (e.g., Środoń and MaCarty, 2008; Macht et al., 2011; Akin and Likos, 2014; Mukhopadhyay et al., 2017; Meegoda and Martin, 2018; Zhang et al., 2019), soils (Quirk and Murray, 1999; Ersahin et al., 2006; Pronk et al., 2013; Pentrák et al., 2018), and organic-rich clay rocks (Kennedy et al., 2002; Kennedy and Wagner, 2011; Kennedy et al., 2014; Derkowski and Bristow, 2012; Saidian et al., 2016). It is widely accepted as the most effective and feasible method for TSSA analysis.

* Corresponding author at: Guangzhou Institute of Geochemistry, CAS, 511 Kehua St. Wushan, Guangzhou 510640, China.
E-mail address: liudong@gig.ac.cn (D. Liu).

https://doi.org/10.1016/j.clay.2019.105190
Received 5 May 2019; Received in revised form 16 June 2019
Available online 02 July 2019

However, the measurement of TSSA in soils and clay-rich rocks has been demonstrated to be affected by the presence of organic matter (OM). For instance, partitioning can occur between EGME and some macromolecular compounds of soil OM, resulting in unreasonably high TSSA values (Chiou et al., 1993; de Jonge and Mittelmeijer-Hazeleger, 1996; Heister, 2014). In addition, as reported by Derkowski and Bristow (2012), detection of TSSA using the EGME adsorption method became very difficult when the OM content was above 3% in shale samples or in an even lower content in OM-bearing smectite. This was due to a chemical reaction between the EGME and sedimentary OM. OM in soil and rocks is usually combined with clay minerals to form a clay-organic matter (clay-OM) complex. Clay-OM complexes are complicated structures that include various occurrence modes of OM. The TSSA detection of the clay-OM complexes may be affected by the occurrence mode of OM. As reported by Ugochukwu (2017), the TSSA of clay-OM complexes were significantly lower than that of original clay minerals. They speculated that this decrease was attributed to the occurrence of intercalated hydrophobic OM that hindered hydrophilic EGME access to the interlayer surface. In our previous studies, the influence of OM occurrence sites on EGME adsorption behavior of clay-OM complexes was investigated. OM in the interlayer space of montmorillonite showed significant interference in EGME adsorption behavior and decreased the EGME adsorption capacity of such a clay (Bu et al., 2019). However, why and which feature of such an OM in interlayer space of montmorillonite would elicit such a strong interruption of EGME adsorption remains unclear.

The adsorption behaviors of guest molecules on OM primarily depend on the content and the type of functional groups of the OM, such as the chain length of the OM molecules. Moreover, the presence of OM with different amounts of alkyl chain and different contents in the interlayer space of montmorillonite will lead to changes in the microstructure and surface properties (i.e., hydrophilic/hydrophobic) of complexes (Wang et al., 2004; He et al., 2006; Lagaly et al., 2006; Zhou et al., 2007; Frost et al., 2008). This may result in some changes in the EGME adsorption behavior. In this case, content and alkyl chain length of interlayer OM may play a key role in the further evaluation of TSSA.

Therefore, the purpose of the present research is to investigate the influence of OM content and alkyl chain length of interlayer OM on the EGME adsorption behaviors of clay-OM complexes and to identify the possible factors that affect the TSSA evaluation of some organic-rich clay rocks. The expandable clay mineral montmorillonite was chosen along with model organic molecules with various chain lengths, such as the short alkyl chain OM tetramethylammonium bromide (TMAB, $(CH_3)_4N(Br)$) and the long alkyl chain OM dodecyl trimethylammonium bromide (DTAB, $CH_3(CH_2)_{11}N(CH_3)_3Br$). These were used to prepare the interlayer clay-OM complexes. An EGME adsorption experiment was then conducted on Mt, OM, and clay-OM complexes. The structural characteristics of the Mt-OM complexes were studied before and after EGME adsorption using X-ray diffraction (XRD) and Fourier transform infrared spectroscopy to comprehensively investigate the EGME adsorption mechanisms of clay-OM complexes. A nitrogen (N_2) adsorption-desorption analysis was used to characterize the specific external surface area and the corresponding pore structure of the Mt-OM complexes.

2. Experiment

2.1. Materials

Raw montmorillonite (Mt) (with a cationic exchange capacity (CEC) = 110.50 mmol/100 g, measured with hexamminecobalt trichloride) with a purity of 97% was obtained from Inner Mongolia, China. Prior to preparation of the Mt-OM complexes, the Mt. was sodium modified using a repeated treatment with 0.5 mol/L NaCl. Then it was washed with distilled water, freeze-dried and ground into a powder. The chemical compositions (wt%) of the Mt. is showed in Table 1.

Table 1
The chemical compositions of Mt.

Sample	Chemical compositions (% mass)								
	SiO_2	Al_2O_3	Fe_2O_3	CaO	MgO	Na_2O	K_2O	TiO_2	L.O.I.
Mt	63.0	16.2	4.9	0.3	4.6	3.6	0.1	0.4	6.9

L.O.I. denotes loss on ignition.

TMAB (with a purity of 99.0 wt%) and DTAB (99.0 wt%) were purchased from the Sigma-Aldrich, Co. LLC. These chemical reagents were used without further purification. The organics of TMAB and DTAB were selected based on the following considerations. They have similar structures and functional groups (i.e., alkyl chains and ammonium ions), which is conducive to comparative study. In addition, some of functional groups are the important components of soluble organics in organic-rich clay rocks or soils (Li et al., 2015; Zhu et al., 2016). Based on the knowledge of the intercalation chemistry of clay minerals (Lagaly et al., 2013), both TMAB and DTAB can be readily intercalated into the interlayer of Mt. via cation exchange (Xi et al., 2007), allowing the preparation of interlayer Mt-OM complexes. The procedure of the preparation of interlayer Mt-OM complexes was as follows. A desired amount of the organic reagent was dissolved into distilled water, and the solution was stirred at 60 °C for 30 min. Then, 20 g of Mt. was added into the solution and the mixture was stirred at 60 °C for 12 h. Solids in the mixture were filtered, repeatedly washed with distilled water, and then dried and ground into a powder. The amounts of the added organics were 0.5, 1.0 and 2.0 times those of the CEC of the Mt. The resultant Mt-OM complexes were identified and labelled using the types of the organics and the amount of the added organics relative to the CEC of the Mt. (e.g., Mt-$TMAB_{(2.0)}$ referred to as the complex of Mt. and TMAB, where the amount of added TMAB was 2.0 times that of the CEC of the Mt).

2.2. Characterization methods

The OM content in the interlayer Mt-OM complexes was determined using an elemental analysis, that was performed using an Elementar Vario EL III Universal CHNOS elemental analyzer.

The X-ray diffraction (XRD) patterns of samples were recorded on a Bruker D8 Advance diffractometer with a Ni filter and CuKα radiation (λ = 0.154 nm) using a generator voltage of 40 kV and a generator current of 40 mA, with a scan rate of 1° (2θ)/min.

The FTIR spectra of the samples were recorded on a Bruker Vertex-70 FTIR spectrometer. The KBr pressed pellet method was used for the FTIR analysis, whereby KBr pellets were prepared by pressing mixtures of 0.9 mg of the sample powder and 80 mg of KBr. The spectra were collected over a range of 400–4000 cm^{-1} with 64 scans at a resolution of 4 cm^{-1}. The diffuse reflectance infrared Fourier transform was used for the EGME.

N_2 adsorption-desorption isotherms were measured using a Micromeritics ASAP2020 system at liquid-nitrogen temperature. The samples were outgassed at 60 °C for 12 h prior to the measurements. The specific surface area (S_{BET}) of the samples were calculated from the nitrogen adsorption data using the multiple-point Brunauer-Emmett-Teller (BET) method (Brunauer et al., 1938). The pore size distribution (PSD) was obtained using the density function theory (DFT) method (Lowell et al., 2012).

The EGME adsorption experiment was conducted according to the following procedure: Approximately 1.0 g of oven-dried (110 °C for 12 h) sample was soaked in the weighing bottles with 3 mL of liquid EGME, and the slurries were allowed to stand in a dry atmosphere for 30 min. The slurries were then placed in desiccators to equilibrate under conditions already specified (in the presence of a $CaCl_2$-EGME solvate, prepared by adding 20 mL of EGME to 100 g of $CaCl_2$ (dried at

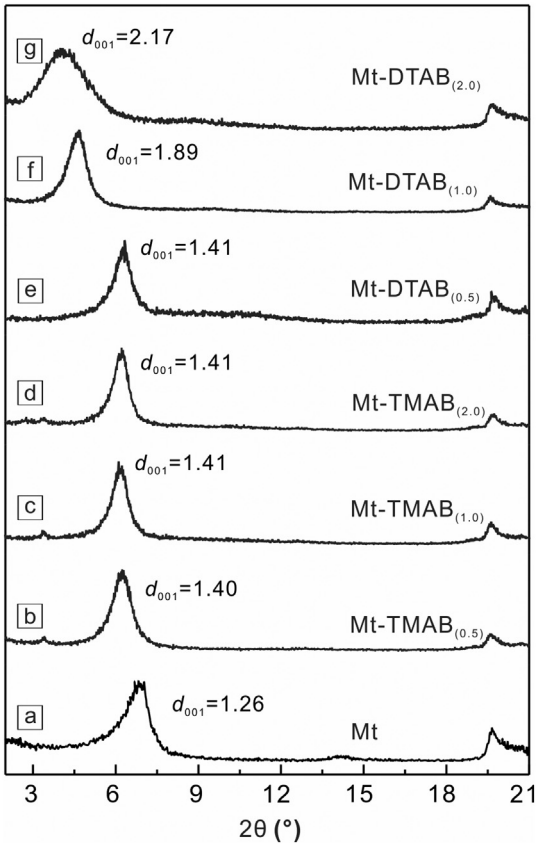

Fig. 1. The XRD patterns of the Mt. and Mt-OM complexes.

80 °C for 12 h in an oven). The desiccator was continually evacuated for 45 min at room temperature and allowed to stand sealed for another hour before air drying. Then, the desiccator was evacuated each day, and the sample was allowed to come to equilibrium. Afterward, the EGME-treated samples were weighed every day, returned to the desiccators and re-equilibrated for further periods until the weight stabilized. The stabilized weight was used to calculate the amount of EGME adsorbed and converted to the SSA of the sample using a conversion factor of 2.86×10^{-4} g/m^2 (Dyal and Hendricks, 1950; Carter et al., 1965; Cerato and Lutenegger, 2002; Yukselen and Kaya, 2006). The resulting EGME-adsorbed samples were differentiated by fixing the sample names with "/EGME". For example, the sample obtained after the TMAB adsorbed the EGME was named TMAB/EGME.

3. Results

3.1. XRD analysis

The XRD patterns of the Mt. and Mt-OM complexes are shown in Fig. 1. The basal spacing (d_{001} values) of each sample obtained from the XRD patterns is listed in Table 1. The d_{001} values of all the Mt-OM complexes are larger than that of the Mt. (1.26 nm (Fig. 1a)). The increase in the d_{001} values represents the enlargement of the interlayer distances of the Mt, which resulted from the replacement of the original interlayer hydrated sodium ions in the Mt. by the intercalated organics (Yuan et al., 2013; Bu et al., 2017). Moreover, the d_{001} values increased with the increasing content of the interlayer OM, which agrees with the results reported by previous studies (Xi et al., 2007; He et al., 2010; Zhu et al., 2017).

For the Mt-TMAB complexes, the value of d_{001} of the Mt-TMAB$_{(0.5)}$ was approximately 1.40 nm (Fig. 1b) corresponding to an interlayer distance of approximately 0.44 nm, which was obtained by subtracting the thickness of the structural layer unit (tetrahedron–octahedron–tetrahedron, TOT, approximately 0.96 nm). However, the d_{001} values of Mt-TMAB$_{(1.0)}$ and Mt-TMAB$_{(2.0)}$ only slightly increased with increased OM contents (TOC%, Table 2, Fig. 1c and d). For the Mt-DTAB complexes with a low content of OM (Mt-DTAB$_{(0.5)}$), the d_{001} value was 1.41 nm. In addition, it was similar to those of the Mt-TMAB complexes (Fig. 1e). At a high OM content, the d_{001} values of Mt-DTAB$_{(1.0)}$ and Mt-DTAB$_{(2.0)}$, 1.89 and 2.17 nm, respectively, were much higher than those of Mt. and all of the Mt-DTAB samples (Fig. 1f and g).

Table 2
The total organic carbon content (TOC) of Mt. and its derivatives and their d_{001} values before and after EGME adsorption.

Samples	[a]TOC (%)	[b]$d_{001(before)}$ (nm)	[c]$d_{001(after)}$ (nm)
Mt	–	1.26	1.48
Mt-TMAB$_{(0.5)}$	3.22	1.40	1.36
Mt-TMAB$_{(1.0)}$	3.98	1.41	1.37
Mt-TMAB$_{(2.0)}$	4.74	1.41	1.38
Mt-DTAB$_{(0.5)}$	9.84	1.41	1.42
Mt-DTAB$_{(1.0)}$	16.61	1.89	2.44
Mt-DTAB$_{(2.0)}$	20.43	2.17	2.72

[a] The total organic carbon content of Mt-OM complexes;
[b] The d_{001} values of samples before EGME adsorption;
[c] The d_{001} values of samples after EGME adsorption.

The basal spacings of the sample after EGME adsorption obtained from XRD patterns (Fig. 2a) are summarized in Table 2. The d_{001} value of the Mt. increased after EGME adsorption, showing the entrance of the EGME into the interlayer space of the Mt. In the Mt-TMAB complexes, there were no significant changes in the d_{001} values after EGME adsorption (Fig. 2a), as reported by previous studies that found that there was no significant increase of the d_{001} values after the tetramethylammonium cations exchanged clays with adsorbed EGME (Chiou and Rutherford, 1997). However, in contrast with the Mt-TMAB complexes and Mt-DTAB complex with low content of OM (Mt-DTAB$_{(0.5)}$), the d_{001} values of the Mt-DTAB complexes with high content of OM, Mt-DTAB$_{(1.0)}$ and Mt-DTAB$_{(2.0)}$, significantly increased after EGME adsorption (Fig. 2b, Table 2).

3.2. Infrared spectroscopy analysis

The assignments of bands of the samples before and after EGME adsorption are summarized in Table 3. These are based on the previous reports of Mt. and alkylammonium organics (Katti et al., 2006; Li et al., 2010; Yuan et al., 2008, 2013). The FTIR spectra of the complexes exhibit vibrations that result from the combination of characteristic bands of Mt. and OM (i.e., DTAB and TMAB) (Fig. 3 and Fig. S1 (Supplementary data)). The weak absorption bands for the Mt-TMAB complexes can be seen at 2962 and 2928 cm^{-1}, and these arise from the asymmetrical stretching of –CH_3 and –CH_2, respectively. The asymmetric bending mode of the head [$(CH_3)_3N^+$-] methyl group at 1488 cm^{-1} appears in the spectra of TMAB and the Mt-TMAB complexes (Fig. 3a and Fig. S1a). Combined with the XRD analysis, the results demonstrate that TMAB molecules were present in the interlayer space of the Mt, as reported by Wang et al. (2004). For DTAB, the characteristic bands at 2918 and 2851 cm^{-1} are –CH_2 asymmetrical and symmetric stretching bands, respectively, and the positions of the bands are sensitive to the conformational characteristics and packing density of the alkyl chains of quaternary ammonium cations (Vaia et al., 1994; Barman et al., 2003; Li and Ishida, 2003; De Paiva et al., 2008). In the Mt-DTAB$_{(1.0)}$, they are located at 2926 and 2854 cm^{-1} (Fig. 3b), compared to 2930 and 2857 cm^{-1} for Mt-DTAB$_{(0.5)}$ and 2923 and 2852 cm^{-1} for Mt-DTAB$_{(2.0)}$ (Fig. S1b).

The characteristic bands of the Mt-OM complexes before and after EGME adsorption were slightly different. In the spectrum of Mt-

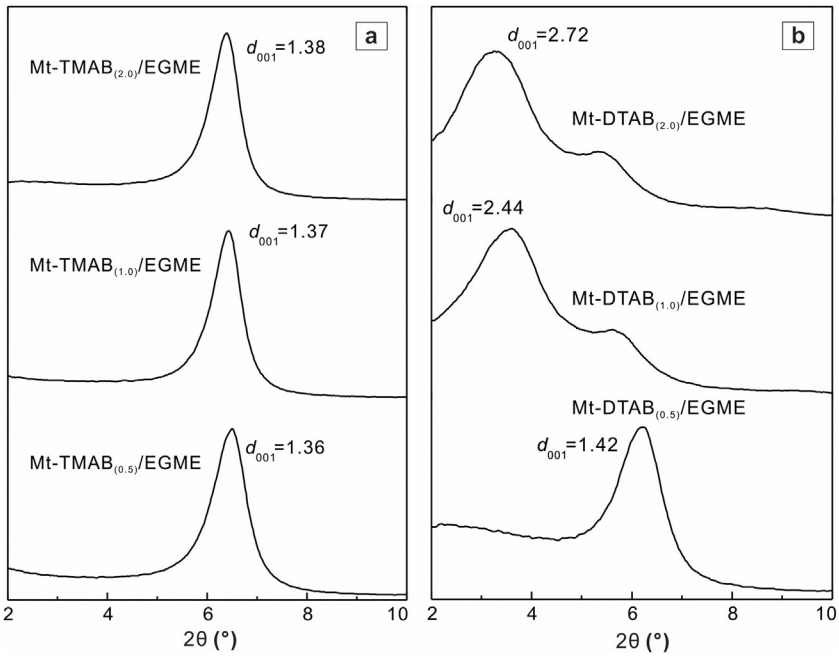

Fig. 2. The XRD patterns of the Mt-OM complexes after treatment with the EGME (a) Mt-TMAB complexes and (b) Mt-DTAB complexes.

Table 3
Vibrations assignments of the FTIR spectra of the samples.

Wavenumber (cm^{-1})	Vibrations
~3627	O—H stretching vibrations
~3619	O—H stretching vibrations of structural hydroxyl groups
~3431/3421	Combination of O—H stretching of water of Mt. and the stretching vibration of the O—H group of the adsorbed EGME hydrogen bonded to the clay surface
~3280	N-H stretching
2985/2962	$-CH_3$ asymmetric stretching
2962	$-CH_3$ asymmetric stretching
2888	$-CH_3$ and $-CH_2$ symmetric stretching
~2928/2949	$-CH_2$ asymmetric stretching
~2854	$-CH_2$ symmetric stretching
~1636	O—H bending vibration
1487/1488	Asymmetric bending mode of the head $[(CH_3)_3N^+$-] methyl group
~1035	Si—O—Si stretching

$TMAB_{(1.0)}$ (Fig. 3a), the OH stretching (~3445 cm^{-1}) shifted to 3431 cm^{-1}, showing a broaden band in the spectrum of Mt-$TMAB_{(1.0)}$/EGME. The band was assigned to a combination of the –OH group stretching of water in Mt. and the stretching vibration of the –OH of EGME that was adsorbed on the clay surface by hydrogen bonds (Dowdy and Mortland, 1968; Nguyen et al., 1987). Moreover, the bending (~1636 cm^{-1}) and stretching (3440 cm^{-1}) vibrations of the interlayer water were significantly weakened, which is attributed to the replacement of the interlayer water by EGME. This result confirms that EGME adsorption occurred in the Mt-TMAB interlayer space. Furthermore, no new-formed bands occurred in the FTIR spectra of TMAB before and after EGME adsorption (Fig. 3a), indicating physical rather than chemical adsorption between the EGME and TMAB molecules. This phenomenon has also been found in other Mt-TMAB complexes (Fig. S2a). Similar to the Mt-TMAB complexes, the spectra of Mt-DTAB before and after EGME adsorption exhibited slight changes (Fig. 3b and Fig. S2b). Therefore, only physical adsorption is believed to have occurred between the EGME and Mt-DTAB complexes.

3.3. Pore structure analysis

The H3-type hysteresis loops appear in all the N_2 adsorption isotherms of the Mt. and Mt-OM complexes, indicating the existence of narrow and slit-like mesopores. These mesopores result from the stacking of the plate-like clay minerals (Thommes et al., 2015; Wang et al., 2016). For the Mt-TMAB complexes, the high N_2 adsorption quantity at a relative pressure near to zero (Fig. 4a and Fig. S3) implies the existence of abundant micropores. This high N_2 adsorption quantity did not occur in the Mt. and Mt-DTAB complexes. This result indicates that the occurrence of interlayer TMAB induced the formation of micropores and these micropores were attributed to the arrangement of TMAB molecules. With an increasing content of TMAB, the micropore size decreased from 0.74 to 0.70 nm (Fig. 4b), but the micropore volumes increased. These features suggest the coexistence of micropores and mesopores in the Mt-TMAB complexes. For the Mt-DTAB complexes, N_2 adsorption began at a higher p/p_0 than that of Mt-TMAB complexes, and N_2 adsorption was primarily present in mesopores. With the increase of the interlayer DTAB content, the N_2 adsorption began at high relative pressure (Fig. 4a), and then the N_2 adsorption capacity decreases, accordingly.

As is well known, N_2 molecules are prevented in the interlayer space and only very a few ones can enter the space by adsorbed water molecules (Liu et al., 2013; Heister et al., 2014), and therefore the S_{BET} of Mt. was only 76.0 m^2/g (Table 4). The S_{BET} values followed the order of Mt-TMAB > Mt. > Mt-DTAB. For the Mt-TMAB complexes, interlayer TMAB molecules with a short alkyl chain supplied more spaces for N_2 molecules when TMAB replaced Na^+ and the content of the interlayer water decreased, as reported in previous studies. For the Mt-DTAB complexes, interlayer DTAB molecules with long alkyl chains seemed to block the interlayer space and less N_2 molecules could enter the space (Wang et al., 2004; He et al., 2006). With the increase in DTAB, S_{BET} decreased to 4.4 m^2/g for Mt-$DTAB_{(2.0)}$.

The TSSA (S_{EGME}) values of all the samples were much higher than the respective S_{BET} (Table 4), showing the detection of the interlayer space in Mt. S_{EGME} values were calculated using the EGME adsorption capacity. The highest value for Mt. was 817.5 m^2/g among the Mt. and Mt-OM complexes. For the Mt-TMAB complexes, the following order of values was obtained: Mt. > Mt-$TMAB_{(0.5)}$ > Mt-$TMAB_{(1.0)}$ > Mt-

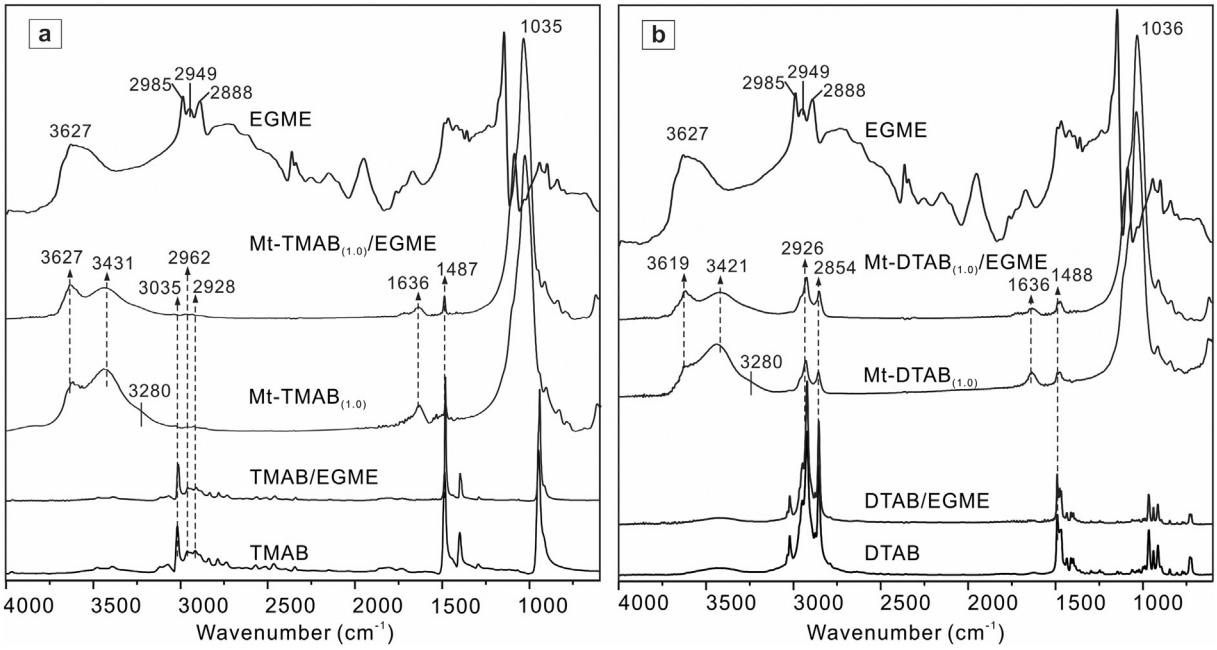

Fig. 3. The IR spectra of the EGME, OM, and Mt-OM complexes before and after EGME adsorption (a) TMAB, Mt-TMAB$_{(1.0)}$, and (b) DTAB, Mt-DTAB$_{(1.0)}$.

TMAB$_{(2.0)}$. The smallest value of 380.8 m^2/g was observed in Mt-TMAB$_{(2.0)}$,which contained the highest TOC (4.74%), one-half that of Mt. (817.5 m^2/g). For the Mt-DTAB complexes, the EGME adsorption capacity order was as follows: Mt. > Mt-DTAB$_{(1.0)}$ > Mt-DTAB$_{(2.0)}$ > Mt-DTAB$_{(0.5)}$. Mt-DTAB$_{(0.5)}$ had the lowest EGME adsorption capacity and thus S_{EGME} value. It must be pointed out that the largest S_{EGME} value was not observed in the Mt-DTAB$_{(0.5)}$ or Mt-DTAB$_{(2.0)}$, which contained the least and the highest OM content, respectively. The largest S_{EGME} value was in the Mt-DTAB$_{(1.0)}$, with a value of 668.2 m^2/g.

Table 4
Mass of the retained EGME, TSSA (S_{EGME}), and N_2-BET SSA (S_{BET}) of the samples.

Sample	Adsorption capacity of EGME (g/g)	S_{EGME} (m^2/g)	S_{BET} (m^2/g)
Mt	0.23	817.5	76.0
Mt-TMAB$_{(0.5)}$	0.13	465.3	147.8
Mt-TMAB$_{(1.0)}$	0.12	411.2	176.2
Mt-TMAB$_{(2.0)}$	0.11	380.8	214.9
Mt-DTAB$_{(0.5)}$	0.13	456.2	23.4
Mt-DTAB$_{(1.0)}$	0.19	668.2	15.2
Mt-DTAB$_{(2.0)}$	0.15	514.3	4.4

4. Discussion

4.1. Influence of interlayer OM on the EGME adsorption behaviors

All d_{001} values of Mt-OM complexes increased after TMAB and DTAB intercalation. However, two types of Mt-OM complexes displayed different d_{001} variation tendencies based on the content of TMAB and DTAB. For three Mt-TMAB complex samples, their interlayer distances were all approximately 0.44 nm. Due to the molecular size of TMAB (Fig. S4a, the height of alkyl-chain is approximately 0.46 nm and the "nailhead" of the alkylammonium cations is 0.51 nm (Zhu et al., 2008)), the distance allowed TMAB molecules to adopt an arrangement of a horizontal monolayer in the interlayer space (Lagaly et al., 2006) (refer to Fig. 5 b-d for a schematic representation of the possible arrangement). For the Mt-DTAB complexes, according to the molecular size of DTAB (Fig. S4b), Mt-DTAB$_{(0.5)}$ followed a monolayer arrangement, because its d_{001} value is approximately 1.41 nm. However, the interlayer distances showed great increases with the increasing content of interlayer DTAB. Therefore, DTAB might adopt an arrangement of a

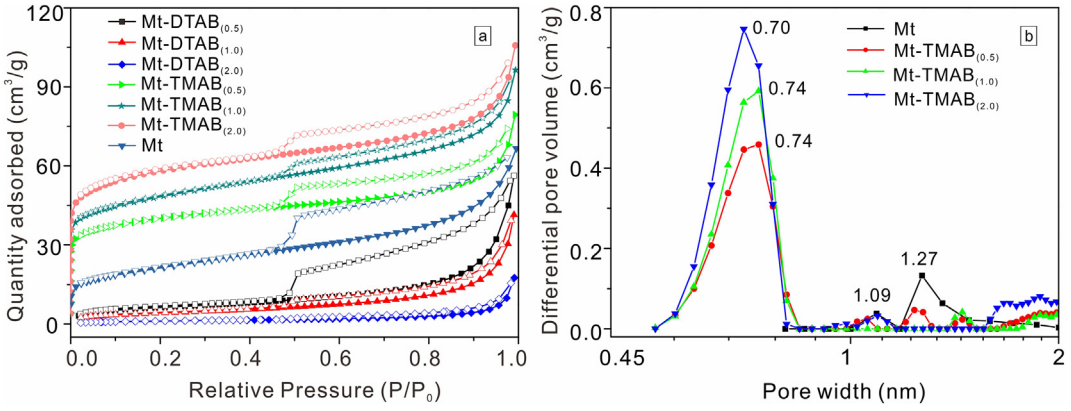

Fig. 4. (a) N_2 adsorption–desorption isotherms of the Mt, Mt-TMAB complexes, and Mt-DTAB complexes; (b) the micro PSD curves of the Mt. and Mt-TMAB complexes.

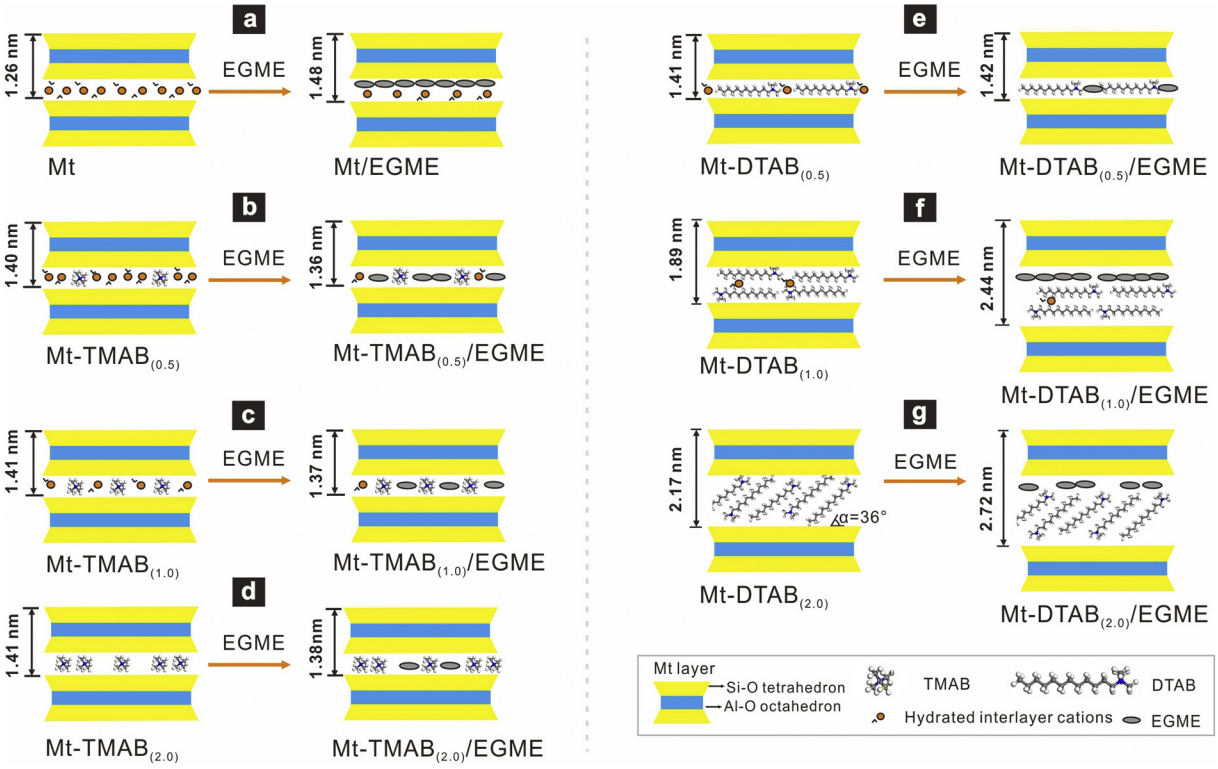

Fig. 5. The possible EGME adsorption mode in Mt. and Mt-OM complexes. (a) Mt, (b) Mt-TMAB$_{(0.5)}$, (c) Mt-TMAB$_{(1.0)}$, (d) Mt-TMAB$_{(2.0)}$, (e) Mt-DTAB$_{(0.5)}$, (f) Mt-DTAB$_{(1.0)}$ and (g) Mt-DTAB$_{(2.0)}$.

lateral bilayer in the interlayer space for Mt-DTAB$_{(1.0)}$ (Fig. 5f) based on the size of DTAB and the stereochemical calculations (for calculation methods, see Lagaly et al. (2006). DTAB might adopt a tilted monolayer arrangement with a tilting angle of 36° for Mt-DTAB$_{(2.0)}$ (Vaia et al., 1994; Lagaly et al., 2006) (Fig. 5g).

Based on the XRD results, the possible arrangements of the EGME molecules in the interlayer space of Mt. are proposed here, as shown in Fig. 5a. According to our previous analysis, the EGME molecules can penetrate into the interlayer space of Mt. by interacting directly with Na^+ ions (Bu et al., 2019). EGME molecules that possess bigger molecular sizes but a lower polar content per unit mass than water replace the interlayer adsorbed water and the d_{001} values of Mt. thus increases. The solvation effect of Na^+ results in a significant lattice expansion of Mt. (Chiou et al., 1993; Chiou and Rutherford, 1997; Quirk and Murray, 1999). As reported by previous studies, d_{001} values after EGME adsorption and the EGME adsorption capacity of montmorillonite and its derivatives, such as Mt-OM complexes are influenced by solvation of interlayer ions and the primary interlayer distances (Chiou and Rutherford, 1997). Solvation of OM is weaker than a metal cation, such as Ca^{2+} and Na^+, and thus, very slight changes in d_{001} values for Mt-TMAB$_{(0.5)}$, Mt-TMAB$_{(1.0)}$, Mt-TMAB$_{(2.0)}$, and Mt-DTAB$_{(0.5)}$ (Table 4). For Mt-DTAB$_{(1.0)}$ and Mt-DTAB$_{(2.0)}$, d_{001} values increased significantly after EGME adsorption and the corresponding EGME adsorption capacity increase due to the latter factor of their large initial interlayer distance, even though the solvation of DTAB was very weak (Table 4). This is because the large initial interlayer distance favors for incremental expansion of Mt. after EGME adsorption, which promote EGME molecules entering into the interlayer space.

The FTIR analysis showed that only physical adsorption was believed to occur between the EGME and Mt-OM complexes when the EGME adsorption reached a equilibrium. EGME adsorption on the Mt-OM complexes possibly consists of the surface adsorption, the filling of pores (including initially accessible pores and interlayer voids created by expansion), and interlayer cation solvation. The pore structure of the Mt-OM complexes with different OM contents and types was distinctly different from each other (Wang et al., 2004; He et al., 2006). Thus, the EGME adsorption capacity and occurrence of EMGE in the interlayer space were affected by the content and arrangement of OM molecules.

In addition to the solvation of interlayer cations and the initial interlayer distance, it is proposed that the arrangement of interlayer OM influenced the d_{001} values. For the Mt-TMAB complexes, some interlayer EGME molecules were speculated to occur in the space that formed between the TMAB molecules (Fig. 5b-d), resulting in nearly constant d_{001} values before and after EGME adsorption (Table 2). As shown in Fig. 4b, abundant micropores with a pore size of approximately 0.74 nm that resulted from interparticle pores of interlayer TMAB provided space for EGME. Thus, the layers were not stretched by the EGME molecules. With the increase of the TMAB content in the narrow interlayer space, the micropores that resulted from the intermolecular spaces of TMAB increased, but the sizes of the newly formed micropores decreased. These micropores allowed N_2 molecules to enter, but some small-sized micropores may prevent EGME molecules from entering, thus increasing the S_{BET} and lowering the adsorption capacity of EGME and S_{EGME} (Table 4). Therefore, although the interlayer distance of each Mt-TMAB sample was similar before and after EGME adsorption, the S_{BET} and S_{EGME} showed some significant variations due to the different arrangements of TMAB with various contents.

Similar to the Mt-TMAB complexes, the arrangement of DTAB in the interlayer space in Mt-DTAB$_{(0.5)}$ displayed a horizontal monolayer based on the XRD results (Table 1). In addition, the EGME molecules seemed to occur in the pores of the intermolecular spaces of DTAB based on the undifferentiated d_{001} values before and after EMGE adsorption (Fig. 5e). This result may be because the intercalated DTAB with a long alkyl chain decreased some preexisting micropores because their S_{BET} values are lower than that of Mt. and are negatively related to the TOC of the complexes (Wang et al., 2004; He et al., 2006) (Table 3). However, Mt-DTAB$_{(1.0)}$ and Mt-DTAB$_{(2.0)}$ possessed a higher DTAB content and larger interlayer distances than Mt-DTAB$_{(0.5)}$, and the

occurrence sites of the EGME molecules were varied, showing a different expansion behaviors of the initial Mt-DTAB complexes (Table 1). For Mt-DTAB$_{(1.0)}$, the EGME molecules showed a lateral bilayer and stacking with the interlayer DTAB layer along the (001) direction (Fig. 5f) based on the XRD result (Table 2). However, the EGME capacity in Mt-DTAB$_{(1.0)}$ was less than that of Mt, although the EGME arrangement was similar in these two samples (Fig. 5a and f). This result may be attributed to the presence of -$(CH_3)_3N^+$. Interlayer EGME molecules were adsorbed on the surface of the montmorillonite layer by hydrogen bonds; however, the $(CH_3)_3N^+$- groups after DTAB intercalation also occupied some adsorbed sites by hydrogen bonds. Therefore, the adsorption capacity of EGME for Mt. decreased when the interlayer DTAB appeared. In addition, more adsorption sites were occupied by DTAB when its arrangement of the tilted monolayer in Mt-DTAB$_{(2.0)}$ occurred. This is because the DTAB molecules that possessed the long alkyl chains in the interlayer space showed a higher ordered mode for the conformation of the alkyl chain and a higher packing density for the arrangement of DTAB with the increase of DTAB content (Li et al., 2010). Thus, the adsorption capacity of Mt-DTAB$_{(2.0)}$ further decreased compared with that of Mt-DTAB$_{(1.0)}$. Therefore, arrangements of the interlayer OM were controlled by the content and alkyl chains, which further influenced EGME adsorption behaviors. The above results indicated that the interlayer OM not only affacted the entry of EGME molecules but also restricted the distribution of EGME between layers.

4.2. Implications for TSSA evaluation of Mt-based samples

The above results seem to describe the possible effect of the occurrence of OM on evaluation of TSSA for some clay-rich samples, especially for some samples with clay-OM nanocomposite. These interlayer organics in expanding clay minerals (i.e., smectite) occupied the interlayer sites, preventing the entering of EGME, which resulted in lower TSSA values. However, the increase of the interlayer OM content did not always decrease the EGME adsorption capacity and TSSA of the samples. These results seem to explain why there was no significant general trend in TSSA values before and after OM removal (e.g., Cihacek and Bremner, 1979; Kennedy et al., 2002; Yukselen-Aksoy and Kaya, 2010). Except for the type of clay minerals (i.e., swelling or non-swelling) (Heister, 2014), these variations have been generally ascribed to the fact that swelling clay minerals tend to form clay-OM nanocomposite (especially the interlayer clay-OM complex) with OM in natural environments. In this case, the types of OM and its association with clay minerals are important factors on evaluation of TSSA of a sample. Different types of OM (i.e., type I or type II kerogen) mean different kinds of functional groups, and so it has been suggested that OM might react with EGME to differing degrees (de Jonge and Mittelmeijer-Hazeleger, 1996; Cornelissen et al., 2005; Derkowski and Bristow, 2012). These current results indicate that the occurrence and arrangement of the interlayer OM could restrict the distribution of EGME molecules and decrease the EGME adsorption capacity. The effects totally depend on the amounts of alkyl chains and contents of the interlayer OM. In addition to the interlayer OM, the OM at the external surface of clay minerals could affect EGME molecules access to the interlayer surface, resulting in lower adsorption capability. Nevertheless, some functional groups showed a high affinity for EGME molecules, resulting in excess uptake of EGME (Bu et al., 2019). Accordingly, the phenomenon seems to indicate that the TSSA of those organic-rich rocks or soils is possibly related to the properties of OM and the arrangement of the interlayer OM. Therefore, bearing in mind the complexity of natural systems, the EGME adsorption method for evaluating the TSSA of rocks that have various swelling clays and soluble organics requires careful use, especially for immature or low maturity source rocks.

5. Conclusions

In this study, the EGME adsorption of OM with different lengths of alkyl chains occurring in the Mt. interlayer space was studied. EGME adsorption capacities and the corresponding TSSA decreased after OM intercalation into interlayer space of Mt, which depends on the OM content and the amounts of alkyl chains. For short alkyl chain OM (TMAB), TSSA values of the Mt-TMAB complexes decreased with the increase of interlayer OM content. However, for long alkyl chain OM (DTAB), TSSA values showed a different variation tendency where the smallest TSSA was not found in the Mt-DTAB complex with the highest DTAB content. The initial interlayer distance and the arrangement of interlayer OM are the primarily factors for EGME adsorption behaviors of the Mt-OM complexes. The large initial interlayer distance favored for incremental expansion of Mt. after EGME adsorption, which promoted EGME molecules entering into the interlayer space. Small initial interlayer distance of Mt-TMAB complexes had low incremental expansion after EGME adsorption and some newly formed micropores in Mt-TMAB complex with high OM content also prevented the EGME molecules from entering, thus lowering the EGME adsorption capacity and TSSA. For Mt-DTAB complexes, although a large initial interlayer distance facilitated the entry of EGME into the interlayer space, more adsorption sites were occupied by the $(CH_3)_3N^+$- groups after DTAB intercalation by hydrogen bonds. The occupation became more significantly when DTAB molecules possessed a higher ordered mode for the conformation of the alkyl chain and a higher packing density for the arrangement of DTAB with the increase of DTAB content. These results demonstrate that EGME adsorption behavior tends to depend on the initial interlayer distance of Mt-OM complexes and the arrangement of interlayer OM. The content and length of the alkyl chains of the interlayer OM could play a significant role in the TSSA evaluation of Mt-based samples. The occurrence of swelling clay minerals deserves more attention when the TSSA of rocks is determined using the EGME adsorption methods in future studies.

Acknowledgements

This work was financially supported by the National Natural Science Foundation of China (Grant Nos. 41802039, 41472044, and 41502031), Youth Innovation Promotion Association CAS for the excellent members (Grant No. 2016-81-01), and Science and Technology Program of Guangzhou, China (Grant No. 201607010280). This is a contribution No. IS-2719 from GIGCAS.

Appendix A. Supplementary data

Supplementary data to this article can be found online at https://doi.org/10.1016/j.clay.2019.105190.

References

Akin, I.D., Likos, W.J., 2014. Specific surface area of clay using water vapor and EGME sorption methods. Geotech. Test. J. 37 (6), 20140064.
Arnepalli, D.N., Shanthakumar, S., Hanumantha Rao, B., Singh, D.N., 2008. Comparison of methods for determining specific-surface area of fine-grained soils. Geotech. Geol. Eng. 26, 121–132.
Barman, S., Venkataraman, N.V., Vasudevan, S., Seshadri, R., 2003. Phase transitions in the anchored organic bilayers of long-chain alkylammonium lead iodides ($C_nH_{2n+1}NH_3$) 2PbI4; n= 12, 16, 18. J. Phys. Chem. B 107 (8), 1875–1883.
Bayat, H., Ebrahimi, E., Ersahin, S., Hepper, E.N., Singh, D.N., Amer, A.-m.M., Yukselen-Aksoy, Y., 2015. Analyzing the effect of various soil properties on the estimation of soil specific surface area by different methods. Appl. Clay Sci. 116-117, 129–140.
Brunauer, S., Emmett, P.H., Teller, E., 1938. Adsorption of gases in multimolecular layers. J. Am. Chem. Soc. 60 (2), 309–319.
Bu, H., Yuan, P., Liu, H., Liu, D., Liu, J., He, H., Zhou, J., Song, H., Li, Z., 2017. Effects of complexation between organic matter (OM) and clay mineral on OM pyrolysis. Geochim. Cosmochim. Ac. 212, 1–15.
Bu, H., Liu, D., Yuan, P., Zhou, X., Liu, H., Du, P., 2019. Ethylene glycol monoethyl ether (EGME) adsorption by organic matter (OM)-clay complexes: Dependence on the OM Type. Appl. Clay Sci. 168, 340–347.

Carter, D.L., Heilman, M.D., Gonzalez, C.L., 1965. Ethylene glycol monoethyl ether for determining surface area of silicate minerals. Soil Sci. 100 (5), 356–360.
Cerato, A.B., Lutenegger, A.J., 2002. Determination of surface area of fine-grained soils by the Ethylene Glycol Monoethyl Ether (EGME) Method. Geotech. Test. J. 25 (3), 315–321.
Chiou, C.T., Rutherford, D.W., 1997. Effects of exchanged cation and layer charge on the sorption of water and EGME vapors on montmorillonite clays. Clay Clay Miner. 45 (6), 867–880.
Chiou, C.T., Rutherford, D., Manes, M., 1993. Sorption of N_2 and EGME vapors on some soils, clays, and mineral oxides and determination of sample surface areas by use of sorption data. Environ. Sci. Technol. 27, 1587–1594.
Cihacek, L.J., Bremner, J.M., 1979. A simplified ethylene glycol monoethyl ether procedure for assessment of soil surface area. Soil Sci. Soc. Am. J. 43 (4), 821–822.
Cornelissen, G., Gustafsson, Ö., Bucheli, T.D., Jonker, M.T., Koelmans, A.A., van Noort, P.C., 2005. Extensive sorption of organic compounds to black carbon, coal, and kerogen in sediments and soils: mechanisms and consequences for distribution, bioaccumulation, and biodegradation. Environ. Sci. Technol. 39 (18), 6881–6895.
de Jonge, H., Mittelmeijer-Hazeleger, M.C., 1996. Adsorption of CO_2 and N_2 on soil organic matter: nature of porosity, surface area, and diffusion mechanism. Environ. Sci. Technol. 30 (12), 408–413.
De Paiva, L.B., Morales, A.R., Díaz, F.R.V., 2008. Organoclays: properties, preparation and applications. Appl. Clay Sci. 42 (1–2), 8–24.
Derkowski, A., Bristow, T.F., 2012. On the problems of total specific surface area and cation exchange capacity measurements in organic-rich sedimentary rocks. Clay Clay Miner. 60 (4), 348–362.
Dowdy, R.H., Mortland, M.M., 1968. Alcohol-water interactions on montmorillonite surfaces: II. Ethylene glycol. Soil Sci. 105, 36–43.
Dyal, R., Hendricks, S., 1950. Total surface of clays in polar liquids as a characteristic index. Soil Sci. 69, 503–509.
Ersahin, S., Gunal, H., Kutlu, T., Yetgin, B., Coban, S., 2006. Estimating specific surface area and cation exchange capacity in soils using fractal dimension of particle-size distribution. Geoderma 136 (3–4), 588–597.
Frost, R.L., Zhou, Q., He, H., Xi, Y., 2008. An infrared study of adsorption of Para-nitrophenol on mono-, di-and tri-alkyl surfactant intercalated organoclays. Spectrochim. Acta Part 69 (1), 239–244.
He, H., Zhou, Q., Martens, W.N., Kloprogge, T.J., Yuan, P., Xi, Y., Zhu, J., Frost, R.L., 2006. Microstructure of $HDTMA^+$-modified montmorillonite and its influence on sorption characteristics. Clay Clay Miner. 54 (6), 689–696.
He, H., Ma, Y., Zhu, J., Yuan, P., Qing, Y., 2010. Organoclays prepared from montmorillonites with different cation exchange capacity and surfactant configuration. Appl. Clay Sci. 48 (1–2), 67–72.
Heister, K., 2014. The measurement of the specific surface area of soils by gas and polar liquid adsorption methods—Limitations and potentials. Geoderma 216, 75–87.
Katti, K.S., Sikdar, D., Katti, D.R., Ghosh, P., Verma, D., 2006. Molecular interactions in intercalated organically modified clay and clay–polycaprolactam nanocomposites: experiments and modeling. Polymer 47 (1), 403–414.
Kennedy, M.J., Wagner, T., 2011. Clay mineral continental amplifier for marine carbon sequestration in a greenhouse ocean. Proc. Natl. Acad. Sci. U. S. A. 108 (24), 9776–9781.
Kennedy, M.J., Pevear, D.R., Hill, R.J., 2002. Mineral surface control of organic carbon in black shale. Science 295 (5555), 657–660.
Kennedy, M.J., Löhr, S.C., Fraser, S.A., Baruch, E.T., 2014. Direct evidence for organic carbon preservation as clay-organic nanocomposites in a Devonian black shale; from deposition to diagenesis. Earth Planet. Sci. Lett. 388 (18), 59–70.
Lagaly, G., Ogawa, M., Dékány, I., 2006. Clay mineral-organic interactions. In: Bergaya, F., Theng, B.K.G., Lagaly, G. (Eds.), Handbook of Clay Science: Developments in Clay Science. vol. 1. Elsevier, Amsterdam, pp. 309–377.
Lagaly, G., Ogawa, M., Dékány, I., 2013. Clay mineral-organic interactions. In: Bergaya, F., Lagaly, G. (Eds.), Handbook of Clay Science: Developments in Clay Science. vol. 5. Elsevier, Amsterdam, pp. 435–505.
Li, Y., Ishida, H., 2003. Concentration-dependent conformation of alkyl tail in the nanoconfined space: hexadecylamine in the silicate galleries. Langmuir 19 (6), 2479–2484.
Li, Z., Jiang, W.T., Chen, C.J., Hong, H., 2010. Influence of chain lengths and loading levels on interlayer configurations of intercalated alkylammonium and their transitions in rectorite. Langmuir 26 (11), 8289–8294.
Li, Y., Cai, J., Song, G., Ji, J., 2015. DRIFT spectroscopic study of diagenetic organic–clay interactions in argillaceous source rocks. Spectrochim. Acta A 148, 138–145.
Liu, D., Yuan, P., Liu, H., Li, T., Tan, D., Yuan, W., He, H., 2013. High-pressure adsorption of methane on montmorillonite, kaolinite and illite. Appl. Clay Sci. 85, 25–30.
Lowell, S., Shields, J.E., Thomas, M.A., Thommes, M., 2012. Characterization of Porous Solids and Powders: Surface Area, Pore Size and Density. vol. 16 Springer Science & Business Media.
Macht, F., Eusterhues, K., Pronk, G.J., Totsche, K.U., 2011. Specific surface area of clay minerals: Comparison between atomic force microscopy measurements and bulk-gas (N_2) and -liquid (EGME) adsorption methods. Appl. Clay Sci. 53, 20–26.
Meegoda, J.N., Martin, L., 2018. In-Situ Determination of specific Surface Area of Clays. Environ. Eng. Geosci. 37, 465–474.
Mukhopadhyay, R., Manjaiah, K.M., Datta, S.C., Yadav, R.K., Sarkar, B., 2017. Inorganically modified clay minerals: Preparation, characterization, and arsenic adsorption in contaminated water and soil. Appl. Clay Sci. 147, 1–10.
Nguyen, T.T., Raupach, M., Janik, L.J., 1987. Fourier-transform infrared study of ethylene glycol monoethyl ether adsorbed on montmorillonite implications for surface area measurements of clays. Clay Clay Miner. 35, 60–67.
Pennell, K.D., Abriola, L.M., Boyd, S.A., 1995. Surface Area of Soil Organic Matter Reexamined. Soil Sci. Soc. Am. J. 59, 1012.
Pentrák, M., Hronský, V., Pálková, H., Uhlík, P., Komadel, P., Madejová, J., 2018. Alteration of fine fraction of bentonite from Kopernica (Slovakia) under acid treatment: a combined XRD, FTIR, MAS NMR and AES study. Appl. Clay Sci. 163, 204–213.
Pronk, G.J., Heister, K., Woche, S.K., Totsche, K.U., Kögel-Knabner, I., 2013. The phenanthrene-sorptive interface of an arable topsoil and its particle size fractions. Eur. J. Soil Sci. 64, 121–130.
Quirk, J.P., Murray, R.S., 1999. Appraisal of the Ethylene Glycol Monoethyl Ether Method for measuring Hydratable Surface Area of Clays and Soils. Soil Sci. Soc. Am. J. 63, 839–849.
Saidian, M., Godinez, L.J., Prasad, M., 2016. Effect of clay and organic matter on nitrogen adsorption specific surface area and cation exchange capacity in shales (mudrocks). J. Nat. Gas Sci. Eng. 33, 1095–1106.
Środoń, J., MaCarty, D.K., 2008. Surface area and layer charge of smectite from CEC and EGME/H_2O-retention measurements. Clay Clay Miner. 56, 155–174.
Thommes, M., Kaneko, K., Neimark, A.V., Olivier, J.P., Rodriguez-Reinoso, F., Rouquerol, J., Sing, K.S.W., 2015. Physisorption of gases, with special reference to the evaluation of surface area and pore size distribution (IUPAC Technical Report). Pure Appl. Chem. 87, 1051–1069.
Ugochukwu, U.C., 2017. Measurement of surface area of modified clays by ethylene glycol monoethyl ether method. Asian J. Chem. 29 (9), 1891–1896.
Vaia, R.A., Teukolsky, R.K., Giannelis, E.P., 1994. Interlayer structure and molecular environment of alkylammonium layered silicates. Chem. Mater. 6 (7), 1017–1022.
Wang, C.C., Juang, L.C., Lee, C.K., Hsu, T.C., Lee, J.F., Chao, H.P., 2004. Effects of exchanged surfactant cations on the pore structure and adsorption characteristics of montmorillonite. J Colloid Interf Sci 280 (1), 27–35.
Wang, Y., Su, X., Xu, Z., Wen, K., Zhang, P., Zhu, J., He, H., 2016. Preparation of surface-functionalized porous clay heterostructures via carbonization of soft-template and their adsorption performance for toluene. Appl. Clay Sci. 363, 113–121.
Xi, Y., Frost, R.L., He, H., 2007. Modification of the surfaces of Wyoming montmorillonite by the cationic surfactants alkyl trimethyl, dialkyl dimethyl, and trialkyl methyl ammonium bromides. J Colloid Interf Sci 305, 150–158.
Yuan, P., Southon, P.D., Liu, Z., Green, M.E., Hook, J.M., Antill, S.J., Kepert, C.J., 2008. Functionalization of halloysite clay nanotubes by grafting with γ-aminopropyltriethoxysilane. The J. Phys. Chem. C 112 (40), 15742–15751.
Yuan, P., Liu, H., Liu, D., Tan, D., Yan, W., He, H., 2013. Role of the interlayer space of montmorillonite in hydrocarbon generation: an experimental study based on high temperature–pressure pyrolysis. Appl. Clay Sci. 75-76, 82–91.
Yukselen, Y., Kaya, A., 2006. Comparison of methods for determining specific surface area of soils. J. Geotech. Geoenviron. 132, 931–936.
Yukselen-Aksoy, Y., Kaya, A., 2010. Method dependency of relationships between specific surface area and soil physicochemical properties. Appl. Clay Sci. 50, 182–190.
Zhang, T., Deng, Y., Cui, Y., Lan, H., Zhang, F., Zhang, H., 2019. Porewater salinity effect on flocculation and desiccation cracking behaviour of kaolin and bentonite considering working condition. Eng. Geol. 251 (1), 11–23.
Zhou, Q., Frost, R.L., He, H., Xi, Y., Liu, H., 2007. Adsorbed Para-nitrophenol on HDTMAB organoclay–a TEM and infrared spectroscopic study. J. Colloid Interface Sci. 307, 357–363.
Zhu, J., Zhu, L., Zhu, R., Chen, B., 2008. Microstructure of organo-bentonites in water and the effect of steric hindrance on the uptake of organic compounds. Clay Clay Miner. 56 (2), 144–154.
Zhu, J., Zhang, P., Qing, Y., Wen, K., Su, X., Ma, L., Wei, J., Liu, H., He, H., Xi, Y., 2017. Novel intercalation mechanism of zwitterionic surfactant modified montmorillonites. Appl. Clay Sci. 141, 265–271.
Zhu, X., Cai, J., Liu, W., Lu, X., 2016. Occurrence of stable and mobile organic matter in the clay-sized fraction of shale: significance for petroleum geology and carbon cycle. Int. J. Coal Geol. 160-161, 1–10.